Annals of Biomedical Engineering, Vol. 22, pp. 23–33, 1994
Printed in the USA.

0090–6964/94 $10.50 + .00

Electrical Properties of Implant Encapsulation Tissue

WARREN M. GRILL and J. THOMAS MORTIMER

Applied Neural Control Laboratory, Department of Biomedical Engineering, Case Western Reserve University, Cleveland, OH

Abstract—The purpose of this study was to determine the electrical properties of the encapsulation tissue that surrounds electrodes chronically implanted in the body. Two four-electrode arrays, fabricated from either epoxy or silicone rubber, were implanted in each of six adult cats for 82 to 156 days. *In vivo* measurements of tissue resistivity using the four-electrode technique indicated that formation of the encapsulation tissue resulted in a significant increase in the resistivity of the tissue around the arrays. *In vitro* measurements of tissue impedance using a four-electrode cell indicated that the resistivity of the encapsulation tissue was a function of the tissue morphology. The tight layers of fibroblasts and collagen that formed around the silicone rubber arrays had a resistivity of 627 ± 108 Ω-cm (mean ± SD; n = 6), which was independent of frequency from 10 Hz to 100 kHz, and was significantly larger than the resistivity of the epoxy encapsulation tissue at all frequencies between 20 Hz and 100 kHz. The combination of macrophages, foreign body giant cells, loose collagen, and fibroblasts that formed around the epoxy arrays had a frequency-dependent resistivity that decreased from 454 ± 123 Ω-cm (n = 5) to 193 ± 98 Ω-cm between 10 Hz and 1 kHz, and was independent of frequency between 1 kHz and 100 kHz, with a mean value of 195 ± 88 Ω-cm. The results indicate that the resistivity of the encapsulation tissue is sufficient to alter the shape and magnitude of the electric field generated by chronically implanted electrodes.

Keywords—Electrical impedance, Resistivity, Conductivity, Electrodes, Neural prostheses.

INTRODUCTION

Electrical activation of the nervous system is a technique to restore function to neurologically impaired persons. Stimulation of intact lower motor neurons provides hand grasp for quadriplegics (27) and standing and walking for paraplegics (20). Stimulation of the auditory nerve allows sensorineural deaf persons to hear (34), and stimulation of the visual cortex produces phosphenes in the visual field of blind persons (5,6). These applications require electrodes that are permanently implanted in the body; however, growth of encapsulation tissue around implanted electrodes may modify the paths of current flow and thus alter the recruitment properties of chronically implanted electrodes.

The body reacts to an implanted electrode with an inflammatory response that leads to formation of a fibrous tissue capsule around the implant. The thickness and cellular morphology of the encapsulation tissue are functions of the shape of the implant (22,41), the surface texture of the implant (39), and the materials from which it is fabricated. A biocompatible implant will be surrounded by a thin, tightly packed layer of fibroblasts, collagen, and occasional macrophages. If the implant is not biocompatible, the tissue response will consist of large numbers of macrophages and foreign body giant cells surrounded by a looser matrix of collagen and fibroblasts (23,38).

Changes in the recruitment properties of chronically implanted electrodes have been attributed to growth of the fibrous tissue capsule. Formation of the encapsulation tissue reduced the efficacy of spinal cord stimulation for relief of chronic pain (26,28,30), changed the signal-to-noise ratio of recordings of nerve compound action potentials (17), and decreased the selectivity and increased the length dependence of epimysial electrodes (14). The geometry of the encapsulation tissue was correlated with the ability or inability to produce unidirectionally propagating action potentials with chronically implanted cuff electrodes (21), and a recent modeling study confirmed that the shape and magnitude of the electric field generated by nerve cuff electrodes are altered by the presence of the encapsulation tissue (7,8).

On the basis of the tight cellular structure of the encapsulation tissue and the reported changes in the recruitment properties of chronically implanted electrodes, we hypothesized that growth of the encapsulation tissue generated a significant barrier to current flow from implanted electrodes. The goals of this work were to determine the effect of growth of the encapsulation on the resistivity of the tissue around an implanted electrode and to determine the electrical resistivity of the encapsulation tissue as a function of frequency. Some results of this study have been published in abstract form (16).

Acknowledgment—This work was supported by National Institutes of Health (NIH) Grant NS-26474 and an NIH Training Grant in Systems and Integrative Biology GM-07535.

Address correspondence to Dr. J. Thomas Mortimer, Applied Neural Control Laboratory, C.B. Bolton Building, Room 3480, Case Western Reserve University, Cleveland, Ohio 44106-4912.

(Received 9/15/92; Revised 6/15/93; Accepted 6/15/93)

METHODS

The goals of this study were addressed in two separate phases. A chronic study was first conducted to measure *in vivo* the effect of growth of the encapsulation tissue on the resistivity of the tissue around chronically implanted electrodes. At the conclusion of the chronic study, a set of terminal acute experiments were conducted to measure *in vitro* the electrical resistivity of the encapsulation tissue as a function of frequency. Animal care and experimental procedures were according to the guidelines set forth in the National Institutes of Health publication *Guide for the Care and Use of Laboratory Animals* and were approved by the Institutional Animal Care and Use Committee of Case Western Reserve University.

In the chronic phase of the study, two four-electrode arrays were implanted using aseptic technique in each of six adult cats under gaseous anesthesia (1–2% halothane and 30% nitrous oxide in oxygen). The arrays were placed in subcutaneous pockets formed by blunt dissection over the loins and sutured to the underlying fascia, with the electrode contacts facing inward, away from the skin. Measurements of the resistivity of the tissue surrounding the implanted electrodes were made at regular intervals using the four-electrode technique.

The arrays were surgically explanted in an acute procedure after a period ranging from 82 to 156 days. Animals were anesthetized with ketamine hydrochloride (30 mg/kg, IM) and atropine (0.044 mg/kg, IM). A venous catheter was installed, and bolus injections of sodium pentobarbital were administered as needed to maintain the proper level of anesthesia. The animals were intubated and body temperature was maintained at 38°C with a heating pad. Samples of encapsulation tissue were removed from the arrays, and measurements of the impedance of the encapsulation tissue were made within 15 minutes using a four-electrode cell.

Implantable Four-Electrode Arrays

A planar array of four electrodes was designed to implement the four-electrode technique in a chronic preparation (Fig. 1). Arrays fabricated from two different substrate materials were used in the chronic study, and in both cases the electrodes were recessed (approximately 150 μm) within the substrate. Recession of the electrodes minimizes electrode polarization resulting from applied currents entering and leaving the voltage sensing electrodes (36). Each of the first six arrays (two arrays/cat, three cats) consisted of four circular 0.5-mm diameter stainless steel electrodes (316 LVM; Goodfellow Metals, Malvern, PA) embedded in a molded epoxy substrate (HYSOL C8-W795 casting compound mixed 4:1 by weight with H-W796 hardener; Dexter Corp., Olean, NY). The epoxy arrays were molded in two sizes, both 1-mm thick, with

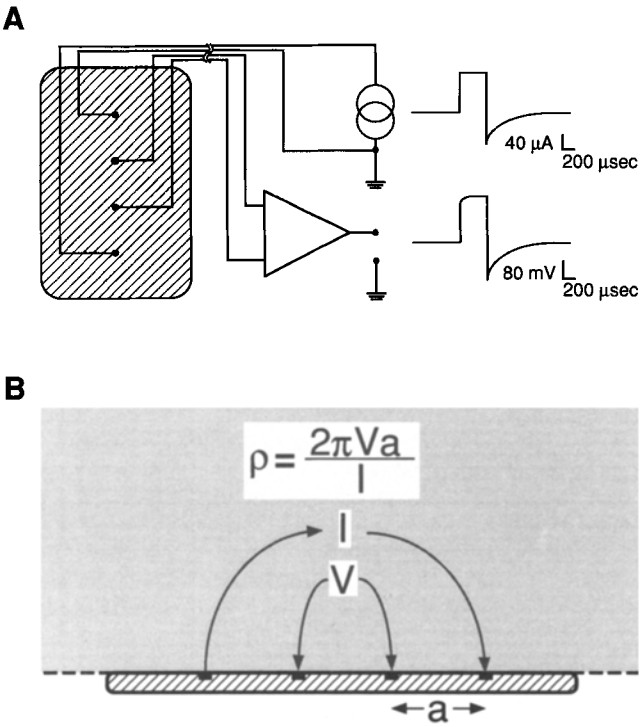

FIGURE 1. The four-electrode technique was implemented *in vivo* to measure the resistivity of the tissue around chronically implanted electrode arrays. (A) Measurements of the resistivity of the tissue around the arrays were made by applying a biphasic current pulse between the outer two electrodes on the array and measuring differentially the induced voltage with the inner pair of electrodes. The electrode arrays consisted of either four stainless steel electrodes molded in an epoxy substrate or four platinum electrodes molded in a silicone rubber substrate with a coiled, Teflon-insulated, multistranded stainless steel lead wire welded to each electrode in the array. (B) The d.c. resistivity of the tissue around the array was calculated from the steady-state magnitude of the voltage response using the solution to Poisson's equation in a homogeneous, semi-infinite medium.

2-mm spacing between the centers of the electrode contacts. The larger epoxy arrays were 1.5-cm wide × 2.5-cm long, and the smaller epoxy arrays were 1.0-cm wide × 2.0-cm long. Each of the second six arrays (two arrays/cat, three cats) consisted of four 35-μm thick platinum foil electrodes (Johnson Mathey, Pittsburgh, PA) molded within a silicone rubber substrate (SILASTIC MDX 4-4210 elastomer mixed 10:1 by weight with MDX 4-4210 curing agent; Dow Corning, Midland, MI). A hoop of stainless steel wire was also embedded within the substrate during molding to maintain the otherwise flexible array in a planar configuration. The silicone rubber arrays were 1.5-cm wide, 2.5-cm long, 1-mm thick, and had 5-mm spacing between the centers of the circular 1-mm diameter electrode contacts. A helically coiled, Teflon-insulated, seven-strand stainless steel lead wire (AS631; Cooner Wire Co., Chatsworth, CA) was welded to each electrode within the arrays. The lead wires were

tunneled subcutaneously to exit percutaneously between the scapulae and crimped to a multipin connector on a mesh vest worn by the animals.

Before implantation, the electrode arrays with attached lead wires were cleaned and sterilized. They were first soaked overnight in ethanol and then rinsed with fresh ethanol to remove any contaminates that were softened by the soak but remained on the surface. They were next soaked overnight for three nights in three consecutive baths of double-distilled water. Between each bath, the arrays were rinsed with double-distilled water. The epoxy arrays were transferred to sealed glass vials of double-distilled water and sterilized with gamma radiation (1500 Gy from a Cesium-137 source). The silicone rubber arrays were sealed in sterilization tubes (CHEX-ALL, Proper Manufacturing Co., Inc., Long Island City, NY), sterilized with ethylene oxide gas, and allowed to de-gas for at least five days before implantation. At the time of implant, the arrays were rinsed in a solution of 500 mL sterile saline and 1 g sterile cefazolin sodium, a broad-spectrum antibiotic.

Chronic Measurement of Tissue Resistivity In Vivo

Measurements of the resistivity of the tissue around the implanted arrays were made every 1 to 2 days for the first week of the epoxy implants and then every four to seven days thereafter, and were made daily throughout the duration of the silicone rubber implants. A 500 μsec, 0.1 to 0.5 mA, capacitively coupled, regulated current, rectangular biphasic pulse with an exponentially decreasing second phase and no interphase delay (see Fig. 1A) was applied between the outer two electrodes on an array using a battery-powered stimulator constructed in our laboratory. The applied current was monitored by measuring the voltage across a 1 kΩ (± 1%) resistor in series with the current source. Pulses were used because this method did not require a large number of measurements per session, as sinusoidal analysis would have. In addition, because the chronic method did not allow direct measurement of the resistivity of the encapsulation, sinusoidal analysis would have added a great deal of complexity to the measurements without providing additional insight into the properties of the encapsulation. The voltage response was measured using the inner pair of electrodes on the array terminated in a high-input impedance (100 MΩ) differential amplifier, with a gain of 10 (Model 113; EG&G PARC), and displayed on a storage oscilloscope (Tektronix 5113).

The measurement instrumentation was tested with a circuit analogue of the electrodes and tissue, and the voltage measurements had a maximum error of 5%. The circuit model of each electrode consisted of a 10 Ω resistor in series with the parallel combination of a 0.047 μF capacitor and a 2 kΩ resistor, and the circuit model of the tissue consisted of a 150 Ω resistor in series with the parallel combination of an 0.47 μF capacitor and a 51 Ω resistor.

Calculation of Apparent Resistivity

The solution to Poisson's equation in a semi-infinite (with respect to the interelectrode spacing), homogeneous conducting medium was used to calculate the apparent resistivity of the tissues surrounding each array (29):

$$\rho = 2\pi Va/I, \quad (1)$$

where ρ is the resistivity, V is the magnitude of the voltage response measured between the inner two electrodes on the array at the end of the first phase of the current pulse, a is the interelectrode spacing, and I is the current applied between the outer two electrodes on the array (see Fig. 1B). The calculated value of resistivity was not a direct measure of the resistivity of the encapsulation tissue, but was the apparent resistivity arising from contributions from all the tissues around the array, including the encapsulation tissue. In addition, because measurements were made after the induced voltage reached steady-state, the measurements were of DC resistivity. The calculated values of DC apparent resistivity were plotted as a function of time after implantation to determine the effects of the encapsulation process and to compare the results from the different arrays.

Testing of Four-Electrode Arrays

The solution to Poisson's equation (Eq. 1) assumes that the electrodes lie on a semi-infinite homogeneous conducting medium (i.e., that the array substrate acted as an insulating plane of infinite area). A set of experiments was conducted in a saline tank to determine how much of the applied current flowed around the back of the arrays. The difference between the magnitude of the voltage response to a current pulse with an array on the surface of the saline bath and the magnitude of the voltage response with the array immersed in the saline bath was used to determine the amount of current that flowed around the back of the arrays. Only 3.9% ± 1.8% (mean ± SD; n = 12) of the applied current flowed around the back of the arrays, and there were no significant differences in the magnitude of the shunt current with the different arrays. The values of apparent resistivity measured *in vivo* with the small (n = 3) and large (n = 3) epoxy arrays were compared at each time point to confirm that the array substrate acted as an infinite insulating plane *in vivo*. There were no significant differences between the resistivity measured with the small and large epoxy arrays, although the large arrays were 87.5% larger in area. Thus, the assumption that the arrays acted as infinite insulating planes was valid.

The accuracy of the implantable arrays was determined

by measuring the resistivity of electrolyte solutions using the same methods described for the *in vivo* measurements of resistivity (i.e., rectangular current pulses). Accurate measurements of the resistivity of aqueous solutions of sodium chloride (0.1, 0.5, and 1.0 mol/L) were made using the implantable four-electrode arrays. With the arrays placed on the fluid surface, the magnitude of the errors were 2.0% ± 1.8% (mean ± SD; n = 6) and 2.5% ± 1.7% (n = 6) for the silicone rubber and epoxy arrays, respectively. With the arrays submerged in the saline tank, the magnitude of the errors were 3.8% ± 3.1% (n = 6) and 3.2% ± 1.4% (n = 6) for the silicone rubber and epoxy arrays, respectively. Although the arrays had different size electrode contacts and different interelectrode spacings, there were no significant differences between the errors either at the surface (p = 0.6898, unpaired, two-tailed *t*-test) or submerged (p = 0.7187, unpaired, two-tailed *t*-test). Accurate chronic measurements of resistivity were also made with the arrays continually immersed in either 0.1 or 0.5 mol/L NaCl, with a magnitude of error of 3.2% ± 2.9% (n = 4) over a period of 92 days. These results indicate that accurate measurements of resistivity could be made on a chronic basis without problems of electrode polarization.

Measurement of the Electrical Impedance of Encapsulation Tissue In Vitro

A four-electrode cell was fabricated and used to measure *in vitro* the impedance of the encapsulation tissue as a function of frequency (36). The cell provided a constrained geometry so that the complex resistivity of the encapsulation tissue as a function of frequency could be calculated from measurements of impedance. The cell consisted of two cylindrical glass chambers between which the tissue sample was placed (Fig. 2). The two chambers were held together using a stainless steel clamp, and a seal was formed between the two chambers using a rubber o-ring. Wax was used to form a seal between the encapsulation tissue sample and the edges of the two chambers (BONE WAX W-31G; Ethicon Inc., Somerville, NJ). The leak impedance at the junction between the two halves of the cell was determined to be greater than 7 MΩ using a piece of insulating plastic film mounted in the tissue chamber. The current passing electrodes were platinum disks 5 mm in diameter, and the voltage measuring electrodes were chlorided silver wires insulated with Teflon, except at the tips.

The impedance measurements were affected significantly by the presence of bubbles within the cell, and it was difficult to remove reliably all the bubbles present in the cell. When the interior of the cell was coated with a surfactant (tridodecylmethylammonium chloride [TDMAC]; Polysciences Inc., Warrington, PA, Catalog

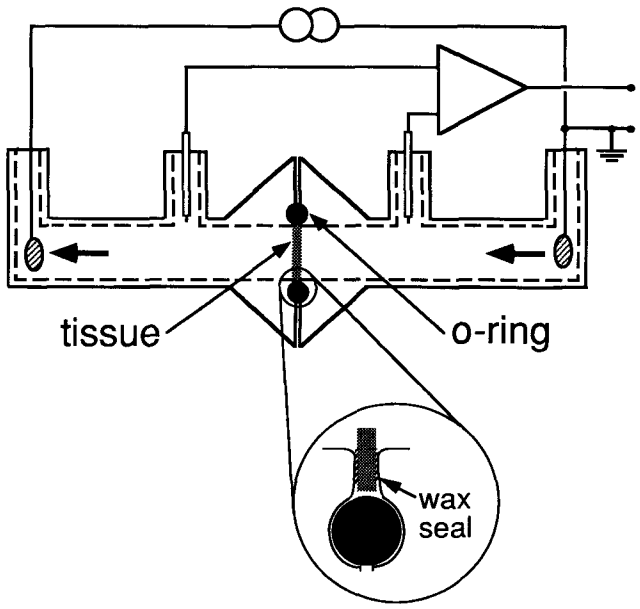

FIGURE 2. Four-electrode cell used for *in vitro* measurement of the impedance of the encapsulation tissue. The cell consisted of two cylindrical glass chambers between which the tissue sample was placed. The junction between the chambers was sealed with an o-ring, and a seal was formed between the tissue sample and the chambers using soft wax. The impedance of the seal was measured to be greater than 7 MΩ. Sinusoidal currents between 10 Hz and 100 kHz were passed between a pair of platinum foil electrodes (*arrows*), and the induced voltage was measured differentially using a pair of Ag-AgCl wire electrodes.

#01595), the number of bubbles formed during filling was greatly reduced, and removal of the bubbles that did form was much easier. The TDMAC was mixed 5 g/L with ethanol, and the cell was soaked in the mixture for 30 minutes. The cell was allowed to dry at room temperature for one hour, and was then washed in five changes of double-distilled water using a vortex stirrer to remove the TDMAC that was not bound to the interior of the cell.

The implanted arrays were surgically exposed at the conclusion of each chronic experiment, and a 1.0 × 1.0 cm piece of the surrounding encapsulation tissue was removed and mounted in the cell. The cell was filled with 0.15 mol/L phosphate-buffered saline (double-distilled H_2O, 150 mmol/L NaCl, 57 mmol/L Na_2HPO_4, 8 mmol/L $NaHPO_4$, with 1 mol/L HCl or 1 mol/L NaOH added to pH 7.4) and was maintained at 37 ± 1°C by immersion in a thermostatically controlled water bath. Sinusoidal currents between 50 and 700 μA were applied between the platinum electrodes, and the resulting voltage was measured differentially with respect to one of the current passing electrodes. The currents were generated using a voltage waveform generator (Wavetek Model 101) and a custom-built voltage to current converter. Current amplitude and phase were monitored by measuring the voltage across a 1 kΩ (±1%) resistor in series with the current source.

The voltage response was measured using a high input impedance (100 MΩ) differential amplifier (Model 113; EG&G PARC) and displayed on a storage oscilloscope (Tektronix 5113). The frequency of the current sinusoids was stepped from 10 Hz to 100 kHz with three steps/decade, and then stepped back down from 100 kHz to 10 Hz to verify the stability of the preparation during a frequency sweep. A complete set of measurements took approximately 6 minutes; during this time, the magnitude of the voltage at a given frequency did not vary by more than 2%. In one preparation, the magnitude of the voltage at 1 kHz decreased by 34% during the course of the measurements. These results were omitted from the data presented herein because a reliable data set was not available for this sample. The measurement system was checked using the same electrical circuit analogue of the electrodes and encapsulation tissue previously described. The maximum errors introduced by the measurement instrumentation were 5 degrees of phase and 7% of magnitude. The phase errors were subtracted from the experimental phase data, and the experimental magnitude data were corrected by dividing the experimental value by the normalized gain.

After the electrical measurements were completed, the tissue samples were fixed in a refrigerated mixture of 2.5% glutaraldehyde and 2.0% paraformaldehyde in 0.1 mol/L sodium cacodylate buffer. Samples for light microscopy were embedded in paraffin, and 3-μm thick sections were cut and stained with Masson's trichrome and hematoxylin and eosin.

Calculation of Resistivity

To determine the voltage drop and phase shift due to the impedance of the tissue, offset voltages and phase angles were measured with the conductivity cell filled with 0.15 mol/L phosphate-buffered saline at 37°C and were subtracted from the values measured with the tissue present in the cell. The thicknesses of the tissue samples used for the *in vitro* measurements were measured after fixation and staining using a calibrated scale (100 μm divisions) under 10× magnification, and were used to calculate the resistivity, $\rho(\mathbf{f})$, from the measured voltages, $V(\mathbf{f})$:

$$\rho(\mathbf{f}) = [V(\mathbf{f}) - V_{os}(\mathbf{f})]\, A/I(\mathbf{f})\, t, \qquad (2)$$

where $\mathbf{f}$ is the sinusoidal frequency, $V_{os}(\mathbf{f})$ is the offset voltage due to the saline solution, A is the cross-sectional area of the tissue sample that was determined by the interior diameter of the cell (0.196 cm^2), $I(\mathbf{f})$ is the applied current, and t is the thickness of the tissue sample.

Testing of Four-Electrode Cell

The linearity and accuracy of impedance measurements made with the four-electrode cell were determined by mounting different numbers of 200-μm thick pieces of filter paper (QUALITATIVE 2, #1002 090; Whatman International Ltd., Maidstone, England) in the tissue chamber and filling the cell with either 0.05 or 0.15 mol/L NaCl at 37°C. The cell was tested using no filter paper, 1 layer, 2 layers, 3 layers, and 4 layers of filter paper. The impedance measured at five different frequencies with the cell filled with 0.15 mol/L NaCl is shown in Fig. 3A as a function of the number of pieces of filter paper in the

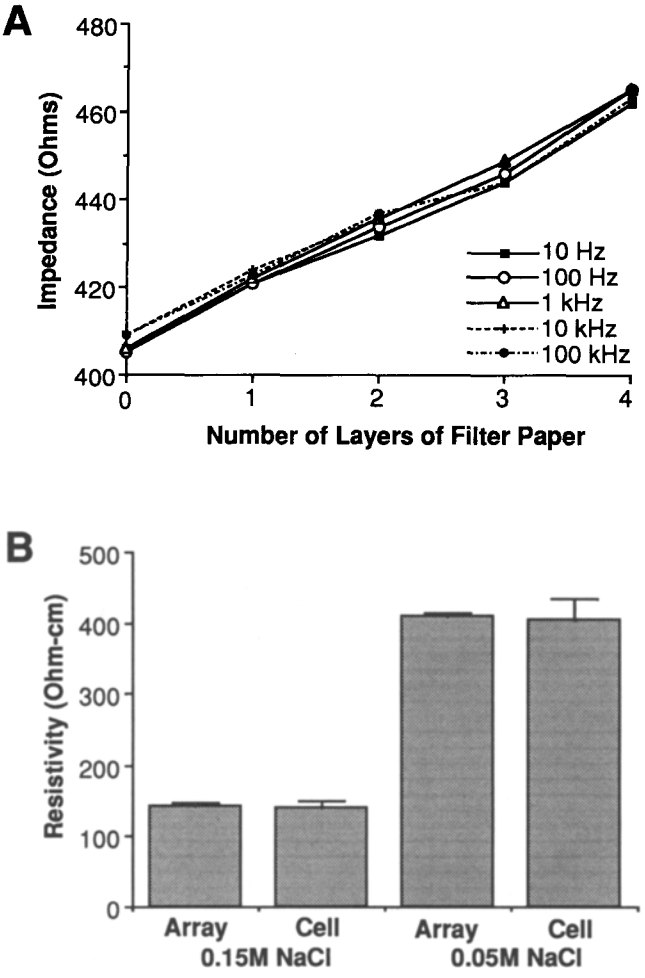

FIGURE 3. Linear and accurate measurements of resistivity with the four-electrode cell over the range of frequencies used in the study of the encapsulation tissue. (A) Impedance measured using the four-electrode cell as a function of the thickness of the filter paper mounted in the tissue chamber at five different frequencies with the cell filled with 0.15 mol/L NaCl at 37°C. The changes in impedance resulting from the addition of more layers of filter paper were measured linearly. (B) A comparison of the resistivity of the saline-impregnated filter paper (mean ± SD) measured using a calibrated implantable four-electrode array (n = 10) and the four-electrode cell (n = 52) filled with either 0.05 or 0.15 mol/L NaCl. There were no significant differences between the values measured using the two methods, indicating that accurate measurements of resistivity were made with the cell.

tissue chamber (i.e., filter paper thickness). As expected, the impedance of the saline-soaked membranes was independent of frequency. Similar results were obtained when the cell was filled with 0.05 mol/L NaCl, but the measured impedance was approximately three times larger than the values measured with 0.15 mol/L NaCl. These data demonstrate that the cell measured linearly changes in impedance over the range of frequencies used in the study of the encapsulation tissue.

Experiments were performed using one of the implantable epoxy arrays to determine the resistivity of the saline-impregnated filter paper. These values of resistivity were compared with those measured using the four-electrode cell to assess the accuracy of the cell (Fig. 3B). A strip of filter paper 2-mm wide, 6-mm long, and 200-μm thick was soaked in either 0.05 or 0.15 mol/L NaCl at 37°C and laid across the electrodes of the array. A 500-μsec current pulse was applied, the induced voltage was measured, and the resistivity of the filter paper was calculated based on the measured voltage and the geometry of the strip. The resistivity of the filter paper measured using the four-electrode array was 144 ± 4 Ω-cm (mean ± SD; n = 10) when soaked in 0.15 mol/L NaCl and 408 ± 5 Ω-cm (n = 10) when soaked in 0.05 mol/L NaCl. These values were larger than those predicted for saline (46 Ω-cm for 0.15 mol/L NaCl and 132 Ω-cm for 0.05 mol/L NaCl), indicating that the filter paper reduced the area of the strip available for conduction as compared with a strip of saline of the same dimensions.

The resistivity of the filter paper was calculated from the *in vitro* cell measurements using Eq. 2, and the resulting value was divided by the number of layers of filter paper. The resistivity of the filter paper was 140 ± 10 Ω-cm (n = 52) with the cell filled with 0.15 mol/L NaCl and 404 ± 29 Ω-cm (n = 52) with the cell filled with 0.05 mol/L NaCl (see Fig. 3B). These values were not significantly different from those determined using the four-electrode array (unpaired, two tailed *t*-test), indicating that the cell measured accurately the resistivity of the filter paper over the range of impedances and frequencies used in this study.

RESULTS

Chronic Changes in Apparent Resistivity

The apparent resistivity of the tissue around the implanted electrode arrays as a function of time after implantation is shown in Figures 4 and 5 for the silicone rubber and epoxy arrays, respectively. The results from the large and small epoxy arrays were lumped together because there was no significant difference between the values of resistivity measured with these two arrays on any given day (see Methods). Chronic results are reported for only four silicone rubber arrays because recurrent lead problems in one animal created an incomplete data set for two of the silicone rubber arrays. The resistivity of the tissue around the arrays 3 to 4 hours after implantation was 353 ± 64 Ω-cm (mean ± SD; n = 6) for the epoxy arrays and 1131 ± 196 Ω-cm (n = 4) for the silicone rubber arrays. A decrease in resistivity was measured during the first 1 to 4 days after implantation to low values of 158 ± 75 Ω-cm (n = 6) and 269 ± 29 Ω-cm (n = 4) for the epoxy and silicone rubber arrays at days 2 and 4, respectively. This decrease corresponded with a 55% decrease in the resistivity of the tissue around the epoxy arrays and a 76%

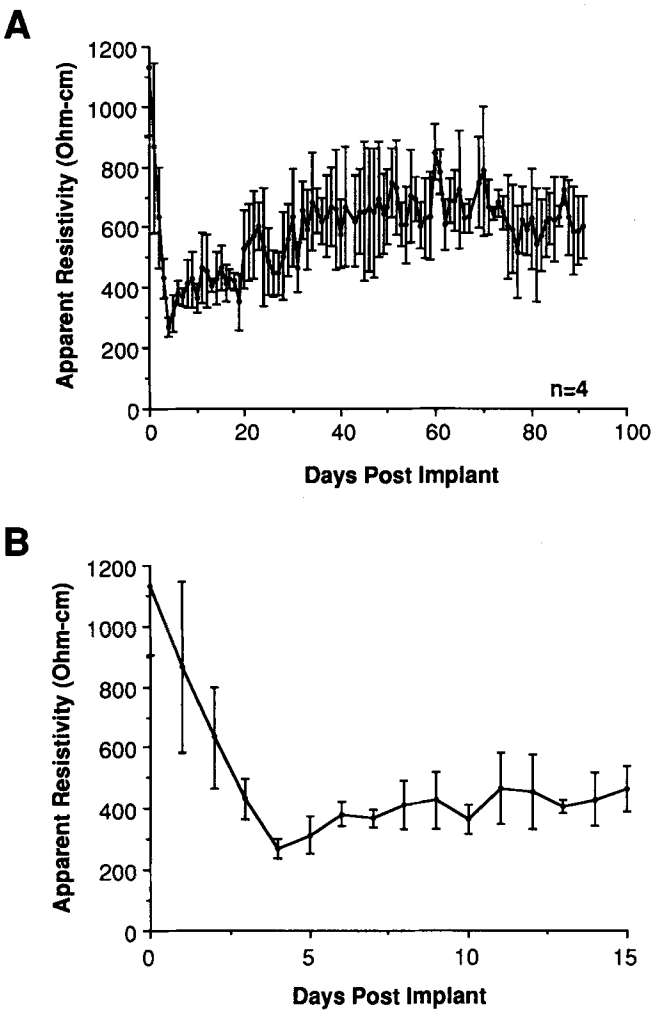

FIGURE 4. Growth of encapsulation tissue led to a significant increase in the resistivity of the tissue around chronically implanted silicone rubber arrays. (A) Apparent resistivity of the tissue around the silicone rubber implants as a function of days post-implant measured using the four-electrode technique (mean ± SD; n = 4). The apparent resistivity increased 148% between day 4 and day 82. (B) Same data from (A) on an expanded time scale illustrates the 76% decrease in resistivity between day 0 and day 4 and shows that the increase in resistivity of the tissue around the silicone rubber arrays began after day 4. The slope of a best-fit line to the resistivity as a function of time curve was significantly greater than zero between days 4 and 15 ($p < 0.002$).

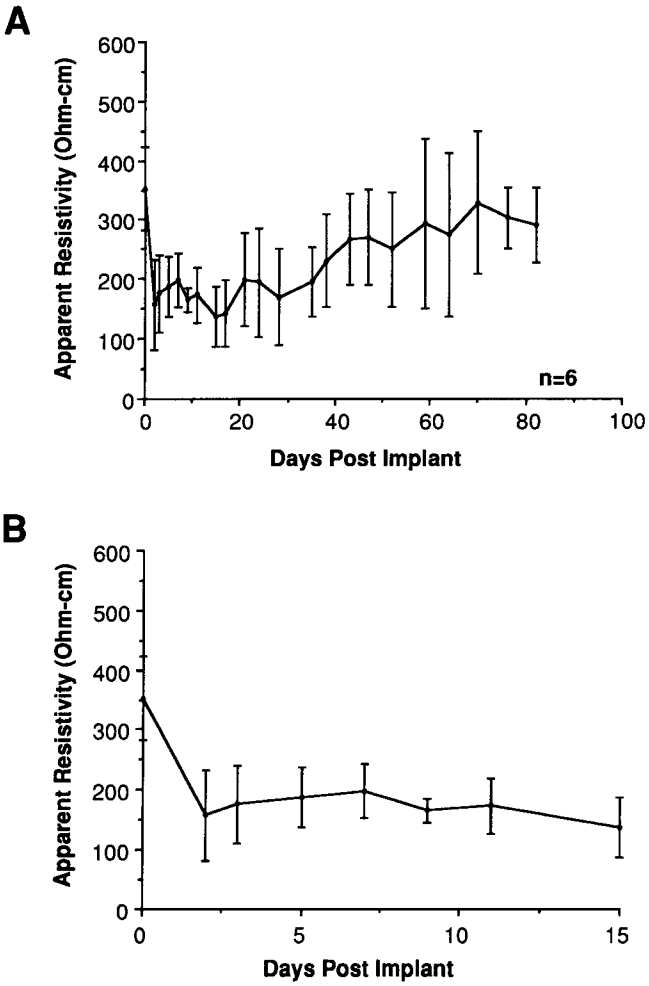

FIGURE 5. Growth of encapsulation tissue led to a significant but delayed increase in the resistivity of the tissue around chronically implanted epoxy arrays. (A) Apparent resistivity of the tissue around the epoxy implants as a function of days post-implant measured using the four-electrode technique (mean ± SD; n = 6). The apparent resistivity increased 88% between day 2 and day 82. (B) Same data from (A) on an expanded time scale illustrates the 55% decrease in resistivity between day 0 and day 2 and shows that the increase in resistivity of the tissue around the epoxy arrays did not begin until after day 15. The slope of a best-fit line to the resistivity as a function of time curve was not significantly greater than zero between days 2 and 15.

decrease in the resistivity of the tissue around the silicone rubber arrays. The initial decrease in resistivity of the tissue around the silicone rubber arrays was followed by a slow increase beginning after day 4 (see Fig. 4B) to a fairly constant value by 40 days after implantation. The mean value of the apparent resistivity of the tissue around the silicone rubber arrays was 666 ± 77 Ω-cm between 60 and 80 days after implantation. This was a significant ($p <$ 0.01; Wilcoxon Rank Sum Test [11]) 148% increase from the lowest value measured 4 days after implantation. The increase in resistivity of the tissue around the epoxy arrays was delayed until after day 15 (see Fig. 5B). The slope of a best-fit line to the resistivity as a function of time curve was not significantly different from zero between days 2 and 15 for the epoxy encapsulation, but was significantly larger than zero for the silicone rubber encapsulation tissue over the same period ($p < 0.002$; unpaired two tailed t-test). The resistivity of the tissue around the epoxy arrays was 298 ± 18 Ω-cm between 59 and 82 days after implantation. This was a significant ($p < 0.05$; Wilcoxon Rank Sum Test) 88% increase from the lowest value measured 2 days after implant.

Resistivity of Encapsulation Tissue

The resistivity and phase shift of the encapsulation tissue from around the arrays are shown in Figure 6 as a function of frequency. The encapsulation tissue from around the epoxy arrays exhibited a frequency-dependent resistivity that decreased significantly ($p < 0.01$; Wilcoxon Rank Sum Test) from 454 ± 190 Ω-cm (mean ± SD; n = 5) to 193 ± 87 Ω-cm as the frequency was increased from 10 to 1 kHz. Between 1 kHz and 100 kHz, the resistivity was 195 ± 88 Ω-cm, with no significant changes in resistivity over this range. The encapsulation tissue from around the epoxy arrays exhibited a small phase lag at lower frequencies and close to zero phase shift above 100 Hz. The resistivity of the encapsulation tissue from around the silicone rubber arrays was independent of frequency, with no significant differences between the resistivity measured at any two frequencies. The mean resistivity of the encapsulation tissue from around the silicone rubber arrays was 587 ± 36 Ω-cm over the whole range of frequencies, and the tissue exhibited close to zero phase shift between 10 Hz and 100 kHz. The resistivity of the encapsulation tissue from around the silicone rubber arrays was significantly larger than the resistivity of the tissue from around the epoxy arrays at all frequencies between 20 Hz and 100 kHz ($p < 0.01$; Wilcoxon Rank Sum Test).

Encapsulation Tissue Morphology

Figures 7A to F are photomicrographs of representative tissue samples taken from the two different types of arrays at the time of explant. The silicone rubber and platinum arrays were surrounded by a tightly packed, well-organized layer of long, thin, parallel fibroblasts and collagen (Fig. 7A,B). There was a layer of 2 to 3 parallel fibroblasts immediately adjacent to the array, with little cytoplasm and small intercellular spaces between adjacent cells (Fig. 7C). The epoxy and stainless steel arrays were surrounded by a layer of macrophages and foreign body giant cells (Fig. 7E), indicative of a chronic foreign body reaction (9). A well vascularized, loose encapsulation layer of disorganized collagen and fibroblasts was present

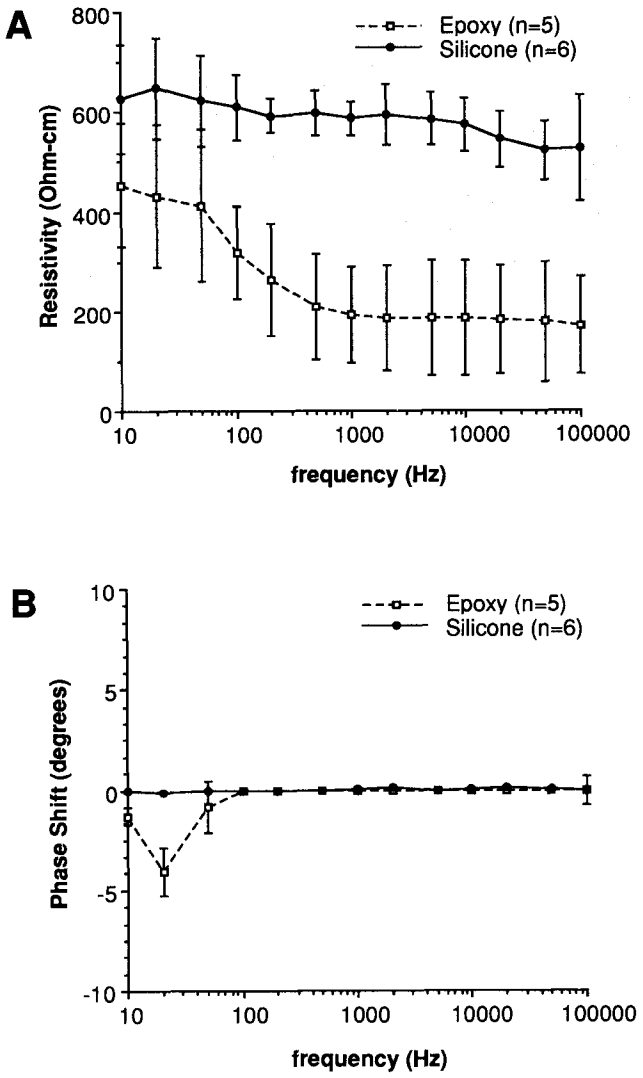

FIGURE 6. The electrical properties of the encapsulation tissue were functions of the tissue structure and hence the biocompatibility of the implanted materials. (A) Resistivity of encapsulation tissue (mean ± SD) from around silicone rubber (n = 6) and epoxy (n = 5) electrode arrays measured *in vitro* using a four-electrode cell. The tight layers of fibroblasts and collagen that formed around the silicone rubber arrays had a resistivity of 627 ± 108 Ω-cm (mean ± SD; n = 6) that was independent of frequency from 10 Hz to 100 kHz and significantly larger ($p < 0.01$) than the resistivity of the epoxy encapsulation tissue at all frequencies between 20 Hz and 100 kHz. The combination of macrophages, foreign body giant cells, loose collagen, and fibroblasts that formed around the epoxy arrays had a frequency-dependent resistivity that decreased from 454 ± 123 Ω-cm (n = 5) at 10 Hz to 193 ± 98 Ω-cm at 1 kHz, where it remained through 100 kHz. (B) Phase angle of encapsulation tissue (mean ± SD) from around silicone rubber (n = 6) and epoxy (n = 5) electrode arrays.

around the layer of foreign body cells (Fig. 7D). There were large intercellular spaces between the cells in the layer of macrophages and foreign body giant cells (Fig. 7F). The thickness of the encapsulation tissue around the epoxy arrays was 808 ± 179 μm (mean ± SD; n = 6), including foreign body cells, collagen, and fibroblasts, and around the silicone rubber arrays was 446 ± 147 μm (n = 6).

DISCUSSION

Growth of encapsulation tissue around implanted electrodes can alter the paths of current flow and thus modify the region of tissue activated by a given stimulus. In the chronic phase of this study, the four-electrode technique was used to eliminate the problems of electrode polarization impedance and to measure accurately changes in resistivity around chronically implanted electrodes. Growth of encapsulation tissue around the implanted electrode arrays led to an increase in the resistivity of the surrounding tissue from 158 to 298 Ω-cm and from 269 to 666 Ω-cm for the epoxy and silicone rubber arrays, respectively. The trend exhibited by the changes in resistivity—a rapid decrease followed by a slow increase—was observed for all arrays in all animals. The timing of the changes in apparent resistivity appears to be consistent with the timing of the events of the encapsulation process, and similar trends have been reported for changes in the impedance and threshold of chronically implanted electrodes (10,19,37). The initial decrease in resistivity over the first one to four days was likely the result of fluid accumulation around the array resulting from an increase in vascular permeability. Fluid exudation is part of the early phase of the body's inflammatory response to an implant (3) and occurs in response to a surgical insult, such as implantation of the array. The increase in resistivity of the tissue around the silicone rubber arrays began after four days; however, the increase in resistivity of the tissue around the epoxy arrays was delayed until after 15 days. The presence of fibroblasts around an implant was observed as early as 24 hours after a wound (31), and the number of fibroblasts began to increase over the next 10 days (9,32). Collagen began to appear within four days after a wound, and its presence increased until the implant was effectively encapsulated (3,32). Formation of the tissue capsule, however, is delayed in the presence of a chronic foreign body response (3,9), as was observed around the epoxy arrays. This process was reflected in the delayed increase in the apparent resistivity of the tissue around the epoxy arrays.

The purpose of the *in vitro* explant experiments was to measure the electrical resistivity of implant encapsulation tissue as a function of frequency. The electrical properties of the encapsulation tissue were found to be a function of the tissue structure and morphology and were thus a function of the biocompatibility of the implant material. The resistivity of the tissue from around the epoxy arrays decreased from 454 to 193 Ω-cm between 10 Hz and 1 kHz, indicating that some current was being conducted across the capacitance of the cell membranes at higher frequen-

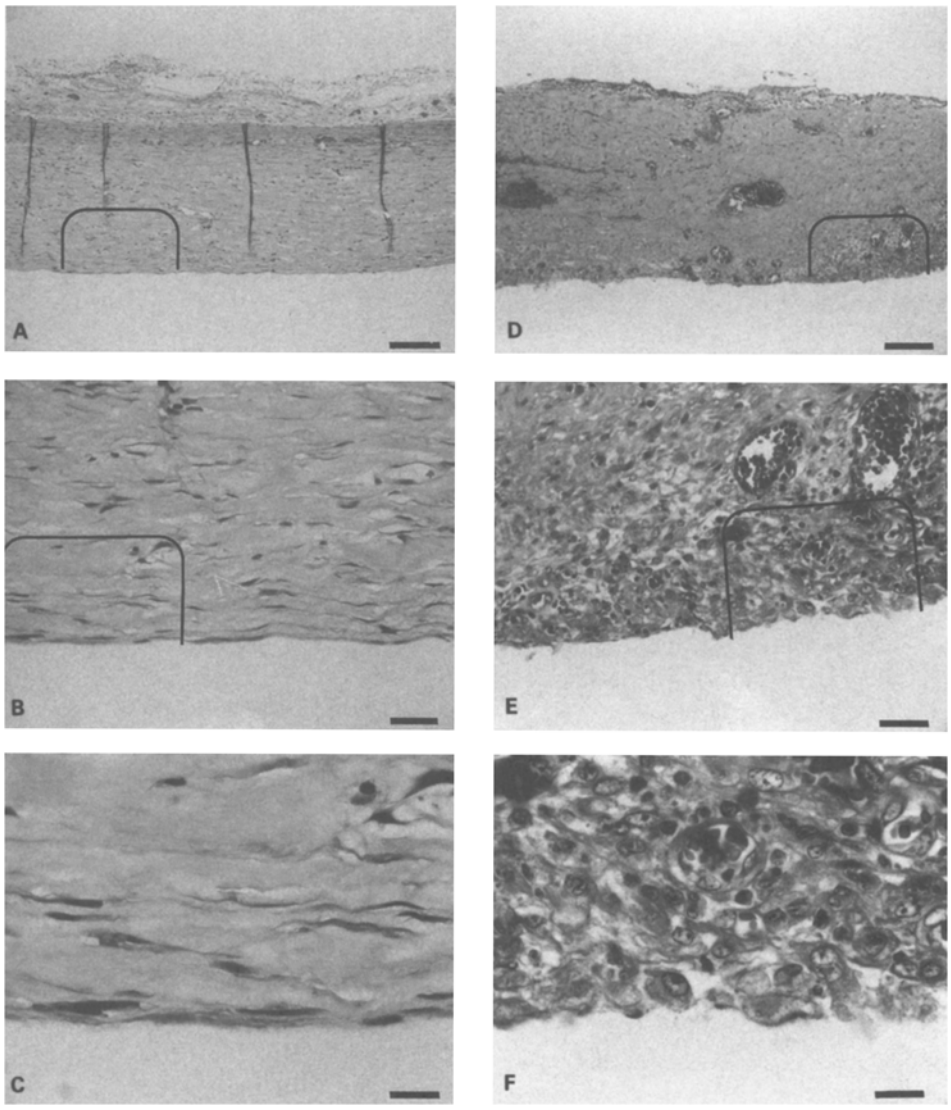

FIGURE 7. The cellular make-up and structure of the encapsulation tissue were functions of the implanted materials. Light micrographs of the encapsulation tissue from around chronically implanted electrode arrays. Fixed tissue samples were embedded in paraffin and 3-μm–thick sections were stained with hematoxylin and eosin. The *black boxes* indicate the regions enlarged in the higher magnification micrographs. (A) Tissue from around a silicone rubber array showing the well organized parallel layers of fibroblasts and collagen and the absence of macrophages and foreign body giant cells (magnification ×76; scale bar = 132 μm). (B) Layers of tightly packed fibroblasts and collagen present around the silicone rubber implants (magnification ×400; scale bar = 25 μm). (C) Tightly packed fibroblasts with little cytoplasm and small interstitial spaces present immediately adjacent to the silicone rubber implants (magnification ×1,000; scale bar = 10 μm). (D) Tissue from around an epoxy array showing the layer of macrophages and foreign body giant cells surrounded by a loose, highly vascularized layer of collagen and fibroblasts (magnification ×76; scale bar = 132 μm). (E) Highly vascularized layers of macrophages and foreign body giant cells present around the epoxy arrays (magnification ×400; scale bar = 25 μm). (F) Macrophages and foreign body giant cells present immediately adjacent to the epoxy implants contain large amounts of cytoplasm and large interstitial spaces (magnification ×1,000; scale bar = 10 μm).

cies (12). This conduction probably occurred through the layer of macrophages and foreign body giant cells, because these cells were not present in the tissue from around the silicone rubber arrays, which exhibited no significant dependence on frequency. A decrease in resistivity between 10 Hz and 1 kHz is typical of biological tissues and is termed *alpha dispersion* (35). The frequency-independent resistivity of the encapsulation tissue from around the silicone rubber arrays (587 Ω-cm) indicates that the current was passing through resistive interstitial pathways (12). The significantly larger value of resistivity measured for the tissue from around the silicone rubber arrays, as compared with the encapsulation from around the epoxy arrays, is consistent with the tighter, more dense

structure of the tissue (compare Figs. 7B and 7E). The resistivity of the tissue from the silicone rubber arrays was slightly larger than the 390 to 560 Ω-cm range reported by Brindley and Lewin (6) for encapsulation tissue from around silicone rubber and platinum electrode arrays implanted on the cortex of baboons. These authors also found that the resistivity of the encapsulation was independent of frequency between 20 Hz and 20 kHz. Finally, the small phase angles measured for both tissues is typical of biological tissues that have conduction pathways through the interstitial space, and thus exhibit a relatively small reactive component of resistivity as compared with the real component of resistivity (1).

Although the arrays were not chronically stimulated, the results of this study are applicable to electrodes that are chronically stimulated at nondamaging levels. Previous studies have demonstrated that there is no significant difference in the encapsulation tissue from around unstimulated electrodes and electrodes stimulated at safe, nondamaging levels (2) and that there is no correlation between the amount of stimulation and the amount of connective tissue growth (4). In addition, the cell types and tissue structure are largely independent of the site of electrode implantation, and the results of this study are applicable for electrodes placed at sites where similar tissue reactions are observed. The encapsulation tissue is similar around intramuscular electrodes (24), epimysial electrodes (14), peripheral nerve electrodes (2,17,25, 37,40), and cortical electrodes (4,6,38). Thus, implantation of unstimulated arrays in the subcutaneous space is adequate to predict the properties of encapsulation tissue around electrodes placed in a number of different locations and stimulated at safe, nondamaging levels.

The results of this study demonstrate that the encapsulation tissue around implanted electrodes provides an additional resistive barrier to current flow and therefore should neither be discounted in applications nor neglected in models of the electrical field generated by chronically implanted stimulating electrodes. The increase in current amplitude required to overcome the effects of the encapsulation tissue may push electrodes into regions where they pass charge through irreversible faradaic reactions. These reactions can lead to electrode corrosion and may release potentially toxic chemical species. An increased resistance due to encapsulation will increase the power required to produce a given current, and the encapsulation will alter the current flow pattern from an electrode with unknown effects on the response to a specific stimulus (18). A recent modeling study (7,8) comparing monopolar and tripolar electrode configurations showed that electrode geometries that have an anode and a cathode on a common substrate are more susceptible to field alterations due to encapsulation tissue than are monopolar electrodes. Such electrodes are being developed for a microinjectable stimulator (42) and for selective activation of peripheral nerves (15,33). A thin layer of high conductivity extracellular fluid (approximately 60 Ω-cm [13]) is present between the implant and the encapsulation tissue (40). This fluid layer provides a low-resistance path between the anode and the cathode, while the encapsulation tissue acts as an additional resistive barrier between the electrodes and the excitable tissue. This process will increase the thresholds of such electrodes and alter the spatial distribution of the electrical field.

REFERENCES

1. Ackmann, J.J.; Seitz, M.A. Methods of complex impedance measurements in biologic tissue. CRC Crit. Rev. Biomed. Eng. 11:281–311; 1984.
2. Agnew, W.F.; McCreery, D.B.; Yuen, T.G.H.; Bullara, L.A. Histologic and physiologic evaluation of electrically stimulated peripheral nerve: considerations for the selection of parameters. Ann. Biomed. Eng. 17:39–60; 1989.
3. Anderson, J.M. Inflammatory response to implants. Trans. Am. Soc. Artif. Int. Organs Vol XXXIV:101–107; 1988.
4. Bartlett, J.R.; Doty, R.W.; Lee, B.B.; Negrao, N.; Overman, W.H. Deleterious effects of prolonged electrical stimulation of striate cortex in macaques. Brain Behav. Evol. 14:46–66; 1977.
5. Bak, M.; Girvin, J.P.; Hambrecht, F.T.; Kufta, C.V.; Loeb, G.E.; Schmidt, E.M. Visual sensations produced by intracortical microstimulation of the human occipital cortex. Med. Biol. Eng. Comput. 28:257–259; 1991.
6. Brindley, G.S.; Lewin, W.S. The sensations produced by electrical stimulation of the visual cortex. J. Physiol. (Lond.) 196:479–493; 1968.
7. Chintalacharuvu, R.R.; Ksienski, D.A.; Mortimer, J.T. A numerical analysis of the electric field generated by a nerve cuff electrode. Proceedings of the Annual International Conference of the IEEE Engineering in Medicine and Biology Society 13:912–913; 1991.
8. Chintalacharuvu, R.R.; Ksienski, D.A.; Mortimer, J.T. A numerical analysis of the electric field generated by a nerve cuff electrode using the finite element method. IEEE Trans. Biomed. Eng. 1994 (in press).
9. Coleman, D.L.; King, R.N.; Andrade, J.D. The foreign body reaction: a chronic inflammatory response. J. Biomed. Mater. Res. 8:199–211; 1974.
10. De Luca, C.J.; Gilmore, L.D.; Bloom, L.J.; Thomson, S.J.; Cudworth, A.L.; Glimcher, M.J. Long-term neuroelectric signal recording from severed nerves. IEEE Trans. Biomed. Eng. 29:393–402; 1982.
11. Devore, J.L. Probability and statistics for engineering and the sciences, ed. 2. Monterey, CA: Brooks/Cole; 1987: pp. 608–614.
12. Eisenberg, R.S.; Mathias, R.T. Structural analysis of electrical properties of cells and tissues. CRC Crit. Rev. Biomed. Eng. 4:203–232; 1980.
13. Geddes, L.A.; Baker, L.E. The specific resistance of biological material—a compendium of data for the biomedical engineer and physiologist. Med. Biol. Eng. 5:271–293; 1967.
14. Grandjean, P.A.; Mortimer, J.T. Recruitment properties of monopolar and bipolar epimysial electrodes. Ann. Biomed. Eng. 14:53–66; 1986.

15. Grill, W.M.; Veraart, C.; Mortimer, J.T. Selective activation of peripheral nerve fascicles: use of field steering currents. Proceedings of the Annual International Conference of the IEEE Engineering in Medicine and Biology Society 13:904–905; 1991.
16. Grill, W.M.; Mortimer, J.T. Electrical impedance of electrode encapsulation tissue. Proceedings of the Annual International Conference of the IEEE Engineering in Medicine and Biology Society 14:1376–1377; 1992.
17. Lefurge, T.; Goodall, E.; Horch, K.; Stensaas, L.; Schoenberg, A. Chronically implanted intrafascicular recording electrodes. Ann. Biomed. Eng. 19:197–207; 1991.
18. Loeb, G.E.; McHardy, J.; Kelliher, E.M.; Brummer, S.B. Neural prostheses. *In:* Williams, D.F.; ed. Biocompatibility in clinical practice, vol II. Boca Raton, FL, CRC Press; 1982: pp. 123–149.
19. Malek, A.M.; Mark, R.G. Functional electrical stimulation for the latissimus dorsi muscle for use in cardiac assist. IEEE Trans. Biomed. Eng. 36:781–788; 1989.
20. Marsolais, E.B.; Kobetic, R. Functional electrical stimulation for walking in paraplegia. J. Bone Joint Surg. [Am] 69-A:728–733; 1987.
21. Martau, J.M. Evaluation of the efficacy and safety of chronic electrical block of the pudenal nerve. M.S. Thesis. Department of Biomedical Engineering. Case Western Reserve University. 1991.
22. Matlaga, B.F.; Yasenchak, L.P.; Salthouse, T.N. Tissue response to implanted polymers: the significance of sample shape. J. Biomed. Mater. Res. 10:391–397; 1976.
23. McNamara, A.; Williams, D.F. The response to the intramuscular implantation of pure metals. Biomaterials 2:33–40; 1981.
24. Mortimer, J.T.; Kaufman, D.; Roessmann, U. Intramuscular electrical stimulation: tissue damage. Ann. Biomed. Eng. 8:235–244; 1980.
25. Naples, G.G.; Mortimer, J.T.; Yuen, T.G.H. Overview of peripheral nerve electrode design and implantation. *In:* Agnew, W.F.; McCreery, D.B.; eds. Neural prostheses: Fundamental Studies. Englewood Cliffs, NJ: Prentice Hall; 1990: pp. 108–145.
26. Nashold, B.S., Jr.; Friedman, H. Dorsal column stimulation for control of pain. J. Neurosurg. 36:590–597; 1972.
27. Peckham, P.H.; Keith, M.W.; Freehafer, A.A. Restoration of functional control by electrical stimulation in the upper extremity of the quadriplegic patient. J. Bone Joint Surg. [Am] 70:144–148; 1988.
28. Pineda, A. Complications of dorsal column stimulation. J. Neurosurg. 48:64–68; 1978.
29. Plonsey, R. Bioelectric phenomena. New York: McGraw-Hill; 1969: pp. 359–360.
30. Reynolds, A.F.; Shetter, A.G. Scarring around cervical epidural stimulating electrode. Neurosurgery 13:63–64; 1983.
31. Robbins, S.L.; Cotran, R.S. Pathologic basis of disease. Philadelphia, PA: W.B. Saunders; 1979: pp. 90–106.
32. Ross, R. Wound healing. Sci. Am. 220:40–50; 1969.
33. Rutten, W.L.C.; van Wier, H.J.; Put, J.H.M. Sensitivity and selectivity of intraneural stimulation using a silicon electrode array. IEEE Trans. Biomed. Eng. 38:192–198; 1991.
34. Schindler, R.A.; Merzenich, M.M.; eds. Cochlear implants. New York: Raven; 1985.
35. Schwan, H.P. Electrical properties of tissue and cell suspensions. *In:* Lawrence, J.H.; Tobias, L.A.; eds. Advances in biological and medical physics, vol. 5. New York: Academic Press; 1957: pp. 147–209.
36. Schwan, H.P. Determination of biological impedance. *In:* Natuk, W.L.; ed. Physical techniques in biological research. New York: Academic Press; 1963: pp. 323–407.
37. Stein, R.B.; Charles, D.; Gordon, T.; Hoffer, J.A.; Jhamandas, J. Impedance of metal electrodes for chronic recording from mammalian nerves. IEEE Trans. Biomed. Eng. 25:532–537; 1978.
38. Stensaas, S.S.; Stensaas, L.J. Histopathological evaluation of materials implanted in the cerebral cortex. Acta Neuropathol. 41:145–155; 1978.
39. Taylor, S.R.; Gibbons, D.F. Effect of surface texture of the soft tissue response to polymer implants. J. Biomed. Mater. Res. 17:205–227; 1983.
40. Thoma, H.; Gerner, H.; Holle, J.; Kluger, P.; Mayr, W.; Meister, B.; Schwanda, G.; Stohr, H. The phrenic pacemaker: substitution of paralyzed functions in tetraplegia. Am. Soc. Artif. Intern. Organs Trans. 10:472–479; 1987.
41. Wood, N.K.; Kaminski, E.J.; Oglesby, R.J. The significance of implant shape in experimental testing of biological materials: disk vs. rod. J. Biomed. Mater. Res. 4:1–12; 1970.
42. Ziaie, B.; Gianchandani, Y.; Najafi, K. A high-current IrOx thin-film neuromuscular microstimulator. Proc. Int. Solid-State Sensors and Actuators. Conf. 124–127; 1992.

Nomenclature

ρ = apparent resistivity of tissue around arrays measured *in vivo*
V = magnitude of the voltage response measured between the inner pair of electrodes on an array
I = magnitude of the current applied between the outer pair of electrodes on an array
a = interelectrode spacing on the array
f = sinusoidal frequency
$\rho(f)$ = resistivity of encapsulation tissue measured *in vitro*
$V(f)$ = voltage response measured with tissue in the cell
$V_{os}(f)$ = offset voltage response measured without tissue in the cell
A = cross-sectional area of the interior of the four-electrode cell
$I(f)$ = current applied between the outer pair of electrodes in the cell
t = thickness of tissue samples measured from fixed and stained samples